We are IntechOpen, the world's leading publisher of Open Access books Built by scientists, for scientists

4,800
Open access books available

122,000
International authors and editors

135M
Downloads

Our authors are among the

154
Countries delivered to

TOP 1%
most cited scientists

12.2%
Contributors from top 500 universities

CLARIVATE ANALYTICS BOOK CITATION INDEX INDEXED

WEB OF SCIENCE™

Selection of our books indexed in the Book Citation Index in Web of Science™ Core Collection (BKCI)

Interested in publishing with us?
Contact book.department@intechopen.com

Numbers displayed above are based on latest data collected.
For more information visit www.intechopen.com

11

Study of Carbon Nanotubes Based on Higher Order Cauchy-Born Rule

Jinbao Wang[1,2], Hongwu Zhang[2], Xu Guo[2] and Meiling Tian[1]
[1]*School of Naval Architecture & Civil Engineering, Zhejiang Ocean University,*
[2]*State Key Laboratory of Structural Analysis for Industrial Equipment,*
Department of Engineering Mechanics, Faculty of Vehicle Engineering and Mechanics,
Dalian University of Technology,
P.R.China

1. Introduction

Since single-walled carbon nanotube (SWCNT) and multi-walled carbon nanotube (MWCNT) are found by Iijima (1991, 1993), these nanomaterials have stimulated extensive interest in the material research communities in the past decades. It has been found that carbon nanotubes possess many interesting and exceptional mechanical and electronic properties (Ruoff et al., 2003; Popov, 2004). Therefore, it is expected that they can be used as promising materials for applications in nanoengineering. In order to make good use of these nanomaterials, it is important to have a good knowledge of their mechanical properties.

Experimentally, Tracy et al. (1996) estimated that the Young's modulus of 11 MWCNTs vary from 0.4TPa to 4.15TPa with an average of 1.8TPa by measuring the amplitude of their intrinsic thermal vibrations, and it is concluded that carbon nanotubes appear to be much stiffer than their graphite counterpart. Based on the similar experiment method, Krishnan et al. (1998) reported that the Young's modulus is in the range of 0.9TPa to 1.70TPa with an average of 1.25TPa for 27 SWCNTs. Direct tensile loading tests of SWCNTs and MWCNTs have also been performed by Yu et al. (2000) and they reported that the Young's modulus are 0.32-1.47TPa for SWCNTs and 0.27-0.95TPa for MWCNTS, respectively. In the experiment, however, it is very difficult to measure the mechanical properties of carbon nanotues directly due to their very small size.

Based on molecular dynamics simulation and Tersoff-Brenner atomic potential, Yakobson et al. (1996) predicted that the axial modulus of SWCNTs are ranging from 1.4 to 5.5 TPa (Note here that in their study, the wall thickness of SWNT was taken as 0.066nm); Liang & Upmanyu (2006) investigated the axial-strain-induced torsion (ASIT) response of SWCNTs, and Zhang et al. (2008) studied ASIT in multi-walled carbon nanotubes. By employing a non-orthogonal tight binding theory, Goze et al. (1999) investigated the Young's modulus of armchair and zigzag SWNTs with diameters of 0.5-2.0 nm. It was found that the Young's modulus is dependent on the diameter of the tube noticeably as the tube diameter is small. Popov et al. (2000) predicted the mechanical properties of SWCNTs using Born's perturbation technique with a lattice-dynamical model. The results they obtained showed that the Young's modulus and the Poisson's ratio of both armchair and zigzag SWCNTs depend on the tube radius as the tube radius are small. Other atomic modeling studies

include first-principles based calculations (Zhou et al., 2001; Van Lier et al., 2000; Sánchez-Portal et al., 1999) and molecular dynamics simulations (Iijima et al., 1996). Although these atomic modeling techniques seem well suited to study problems related to molecular or atomic motions, these calculations are time-consuming and limited to systems with a small number of molecules or atoms.

Comparing with atomic modeling, continuum modeling is known to be more efficient from computational point of view. Therefore, many continuum modeling based approaches have been developed for study of carbon nanotubes. Based on Euler beam theory, Govinjee and Sackman (1999) studied the elastic properties of nanotubes and their size-dependent properties at nanoscale dimensions, which will not occur at continuum scale. Ru (2000a,b) proposed that the effective bending stiffness of SWCNTs should be regarded as an independent material parameter. In his study of the stability of nanotubes under pressure, SWCNT was treated as a single-layer elastic shell with effective bending stiffness. By equating the molecular potential energy of a nano-structured material with the strain energy of the representative truss and continuum models, Odegard et al. (2002) studied the effective bending rigidity of a graphite sheet. Zhang et al. (2002a,b,c, 2004) proposed a nanoscale continuum theory for the study of SWCNTs by directly incorporating the interatomic potentials into the constitutive model of SWCNTs based on the modified Cauchy-Born rule. By employing this approach, the authors also studied the fracture nucleation phenomena in carbon nanotubes. Based on the work of Zhang (2002c), Jiang et al. (2003) proposed an approach to account for the effect of nanotube radius on its mechanical properties. Chang and Gao (2003) studied the elastic modulus and Poisson's ratio of SWCNTs by using molecular mechanics approach. In their work, analytical expressions for the mechanical properties of SWCNT have been derived based on the atomic structure of SWCNT. Li and Chou (2003) presented a structural mechanics approach to model the deformation of carbon nanotubes and obtained parameters by establishing a linkage between structural mechanics and molecular mechanics. Arroyo and Belytschko (2002, 2004a,b) extended the standard Cauchy-Born rule and introduced the so-called exponential map to study the mechanical properties of SWCNT since the classical Cauchy-Born rule cannot describe the deformation of crystalline film accurately. They also established the numerical framework for the analysis of the finite deformation of carbon nanotubes. The results they obtained agree very well with those obtained by molecular mechanics simulations. He et al. (2005a,b) developed a multishell model which takes the van der Waals interaction between any two layers into account and reevaluated the effects of the tube radius and thickness on the critical buckling load of MWCNTs. Gartestein et al. (2003) employed 2D continuum model to describe a stretch-induced torsion (SIT) in CNTs, while this model was restricted to linear response. Using the 2D continuum anharmonic anisotropic elastic model, Mu et al. (2009) also studied the axial-induced torsion of SWCNTs.

In the present work, a nanoscale continuum theory is established based on the higher order Cauchy-Born rule to study mechanical properties of carbon nanotubes (Guo et al., 2006; Wang et al., 2006a,b, 2009a,b). The theory bridges the microscopic and macroscopic length scale by incorporating the second-order deformation gradient into the kinematic description. Our idea is to use a higher-order Cauchy-Born rule to have a better description of the deformation of crystalline films with one or a few atom thickness with less computational efforts. Moreover, the interatomic potential (Tersoff 1988, Brenner 1990) and

the atomic structure of carbon nanotube are incorporated into the proposed constitutive model in a consistent way. Therefore SWCNT can be viewed as a macroscopic generalized continuum with microstructure. Based on the present theory, mechanical properties of SWCNT and graphite are predicted and compared with the existing experimental and theoretical data.

The work is organized as follows: Section 2 gives Tersoff-Brenner interatomic potential for carbon. Sections 3 and 4 present the higher order Cauchy-Born rule is constructed and the analytical expressions of the hyper-elastic constitutive model for SWCNT are derived, respectively. With the use of the proposed constitutive model, different mechanical properties of SWCNTs are predicted in Section 5. Finally, some concluding remarks are given in Section 6.

2. The interatomic potential for carbon

In this section, Tersoff-Brenner interatomic potential for carbon (Tersoff, 1988; Brenner, 1990), which is widely used in the study of carbon nanotubes, is introduced as follows.

$$V(r_{IJ}) = V_R(r_{IJ}) - B_{IJ}V_A(r_{IJ}) \tag{1}$$

Where

$$V_R(r) = f(r)\frac{D_e}{S-1}e^{-\sqrt{2s}\beta(r-r_e)}, \quad V_A(r) = f(r)\frac{D_e S}{S-1}e^{-\sqrt{2/s}\beta(r-r_e)} \tag{2}$$

$$f(r) = \begin{cases} 1 & r < r_1 \\ \frac{1}{2}\left\{1 + cos\left[\frac{\pi(r-r_1)}{(r_2-r_1)}\right]\right\} & r_1 \le r \le r_2 \\ 0 & r > r_2 \end{cases} \tag{3}$$

$$B_{IJ} = \left[1 + \sum_{K(\neq I,J)} G(\theta_{IJK}) f(r_{IK})\right]^{-\delta} \tag{4}$$

$$G(\theta) = a_0\left[1 + \frac{c_0^2}{d_0^2} - \frac{c_0^2}{d_0^2 + (1+cos\theta)^2}\right] \tag{5}$$

with the constants given in the following.

$$D_e = 6.000\ eV, \quad S = 1.22, \quad \beta = 21nm^{-1}, \quad r_e = 0.1390nm$$

$$\delta = 0.50000\ , \quad a_0 = 0.00020813\ , \quad c_0 = 330\ , \quad d_0 = 3.5$$

3. The higher order cauchy-born rule

Cauchy-Born rule is a fundamental kinematic assumption for linking the deformation of the lattice vectors of crystal to that of a continuum deformation field. Without consideration of

diffusion, phase transitions, lattice defect, slips or other non-homogeneities, it is very suitable for the linkage of 3D multiscale deformations of bulk materials such as space-filling crystals (Tadmor et al., 1996; Arroyo and Belytschko, 2002, 2004a,b). In general, Cauchy-Born rule describes the deformation of the lattice vectors in the following way:

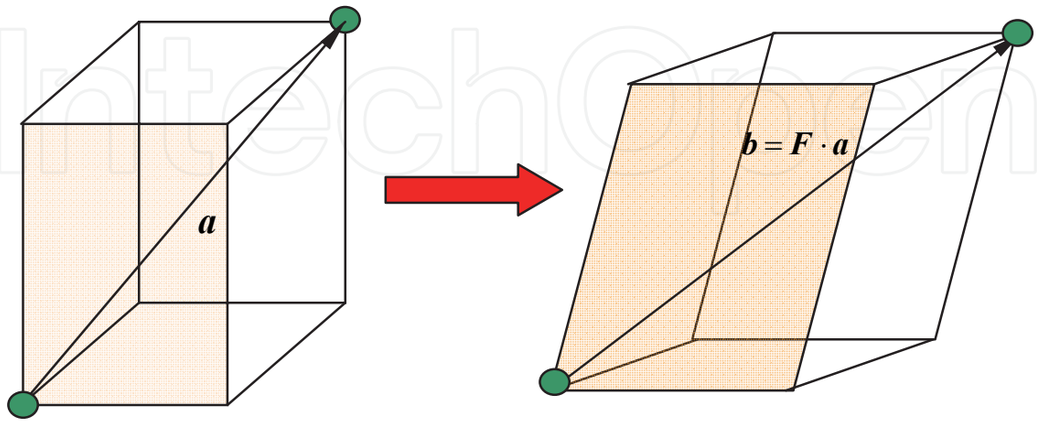

Fig. 1. Illustration of the Cauchy-Born rule

$$\mathbf{b} = \mathbf{F} \bullet \mathbf{a} \tag{6}$$

where $\mathbf{F}$ is the two-point deformation gradient tensor, $\mathbf{a}$ denotes the undeformed lattice vector and $\mathbf{b}$ represents the corresponding deformed lattice vector (see Fig. 1 for reference). In the deformed crystal, the length of the deformed lattice vector and the angle between two neighboring lattice vectors can be expressed by means of the standard continuum mechanics relations:

$$\mathbf{b} = \sqrt{\mathbf{a} \bullet \mathbf{C}\mathbf{a}} \quad \text{and} \quad \cos\theta = \frac{\mathbf{a}' \bullet \mathbf{C}\mathbf{a}}{||\mathbf{b}'||||\mathbf{b}||} \tag{7}$$

where $\mathbf{b}' = \mathbf{F} \bullet \mathbf{a}'$ ($\mathbf{b}'$ and $\mathbf{a}'$ denote the neighboring deformed and undeformed lattice vector, respectively) and $\mathbf{C} = \mathbf{F}^T \bullet \mathbf{F}$ is the Green strain tensor measured from undeformed configuration. θ represents the angle formed by the deformed lattice vectors $\mathbf{b}$ and $\mathbf{b}'$. Though the use of Cauchy-Born rule is suitable for bulk materials, as was first pointed out by Arroyo and Belytschko (2002; 2004a,b), it is not suitable to apply it directly to the curved crystalline films with one or a few atoms thickness, especially when the curvature effects are dominated. One of the reasons is that if we view SWCNT as a 2D manifold without thickness embedded in 3D Euclidean space, since the deformation gradient tensor $\mathbf{F}$ describes only the change of infinitesimal material vectors emanating from the same point in the tangent spaces of the undeformed and deformed curved manifolds, therefore the deformation gradient tensor $\mathbf{F}$ is not enough to give an accurate description of the length of the deformed lattice vector in the deformed configuration especially when the curvature of the film is relatively large. In this case, the standard Cauchy-Born rule should be modified to give a more accurate description for the deformation of curved crystalline films, such as carbon nanotubes.

In order to alleviate the limitation of Cauchy-Born rule for the description of the deformation of curved atom films, we introduce the higher order deformation gradient into the kinematic relationship of SWCNT. The same idea has also been shown by Leamy et al. (2003).

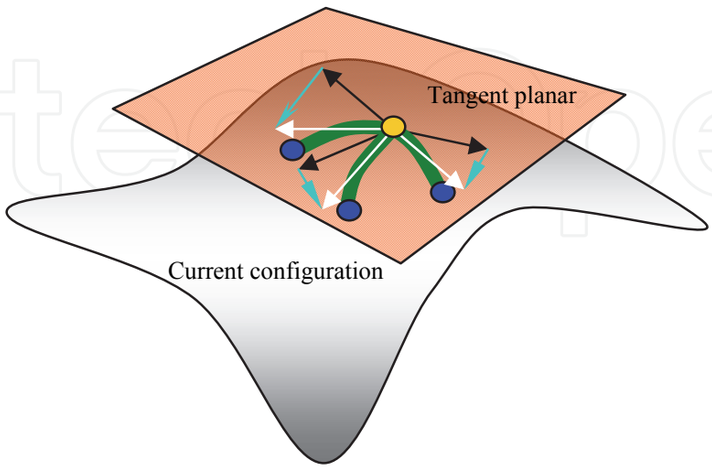

Fig. 2. Schematic illustration of the higher order Cauchy-Born rule

From the classical nonlinear continuum mechanics point of view, the deformation gradient tensor $\mathbf{F}$ is a linear transformation, which only describes the deformation of an *infinitesimal* material line element $d\mathbf{X}$ in the undeformed configuration to an infinitesimal material line element $d\mathbf{x}$ in deformed configuration, i.e.

$$d\mathbf{x} = \mathbf{F} \bullet d\mathbf{X} \tag{8}$$

As in Leamy et al. (2003), by taking the finite length of the initial lattice vector $\mathbf{a}$ into consideration, the corresponding deformed lattice vector should be expressed as:

$$\mathbf{b} = \int_0^{\mathbf{a}} \mathbf{F}(\mathbf{s}) d\mathbf{s} \tag{9}$$

Assuming that the deformation gradient tensor $\mathbf{F}$ is smooth enough, we can make a Taylor's expansion of the deformation field at $\mathbf{s} = \mathbf{0}$, which is corresponding to the starting point of the lattice vector $\mathbf{a}$.

$$\mathbf{F}(\mathbf{s}) = \mathbf{F}(\mathbf{0}) + \nabla \mathbf{F}(\mathbf{0}) \bullet \mathbf{s} + \nabla \nabla \mathbf{F}(\mathbf{0}) : (\mathbf{s} \otimes \mathbf{s}) / 2 + \mathbf{O}(|\,|\mathbf{s}|\,|^3) \tag{10}$$

Retaining up to the second order term of $\mathbf{s}$ in (10) and substituting it into (9), we can get the approximated deformed lattice vector as:

$$\mathbf{b} \approx \mathbf{F}(\mathbf{0}) \bullet \mathbf{a} + \frac{1}{2} \nabla \mathbf{F}(\mathbf{0}) : (\mathbf{a} \otimes \mathbf{a}) \tag{11}$$

Comparing with the standard Cauchy-Born rule, it is obvious that with the use of this higher order term, we can pull the vector $\mathbf{F} \bullet \mathbf{a}$ more close to the deformed configuration (see Fig. 2 for an illustration). By retaining more higher-order terms, the accuracy of

approximation can be enhanced. Comparing with the exponent Cauchy-Born rule proposed by Arroyo and Belytschko (2002, 2004a,b), it can improve the standard Cauchy-Born rule for the description of the deformation of crystalline films with less computational effort.

4. The hyper-elastic constitutive model for SWCNT

With the use of the above kinematic relation established by the higher order Cauchy-Born rule, a constitutive model for SWCNTs can be established. The key idea for continuum modeling of carbon nanotube is to relate the phenomenological macroscopic strain energy density W_0 per unit volume in the material configuration to the corresponding atomistic potential.

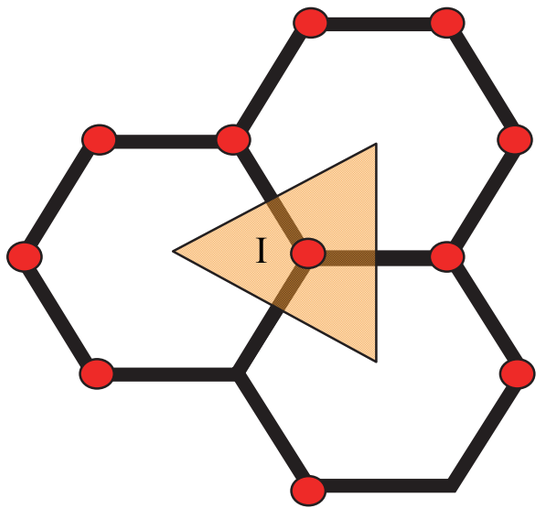

Fig. 3. Representative cell corresponding to an atom I

Assuming that the energy associated with an atom I can be homogenized over a representative volume V_I in the undeformed material configuration (i.e. graphite sheet, see Fig. 3 for reference), the strain energy density in this representative volume can be expressed as:

$$W_0 = W_0(|\mathbf{r}_{I1}|, |\mathbf{r}_{I2}|, |\mathbf{r}_{I3}|) = \sum_{J=1}^{3} V_{IJ}(\mathbf{r}_{I1}, \mathbf{r}_{I2}, \mathbf{r}_{I3})/2V_I = W_0(\mathbf{F}, \mathbf{G}) \tag{12}$$

And

$$\mathbf{r}_{IJ} = \mathbf{F} \bullet \mathbf{R}_{IJ} + \mathbf{G} : (\mathbf{R}_{IJ} \otimes \mathbf{R}_{IJ})/2 \tag{13}$$

where $\mathbf{R}_{IJ}$ and $\mathbf{r}_{IJ}$ denote the undeformed and deformed lattice vectors, respectively. V_I is the volume of the representative cell. $\mathbf{F} = F_{ij}\mathbf{e}_i \otimes \mathbf{e}_j$ and $\mathbf{G} = \nabla\mathbf{F} = G_{ijk}\mathbf{e}_i \otimes \mathbf{e}_j \otimes \mathbf{e}_k$ are the first and second order deformation gradient tensors, respectively. Note that here and in the following discussions, a unified Cartesian coordinate system has been used for the description of the positions of material points in both of the initial and deformed configurations.

Based on the strain energy density W_0, as shown by Sunyk et al. (2003), the first Piola-Kirchhoff stress tensor $\mathbf{P}$, which is work conjugate to $\mathbf{F}$ and the higher-order stress tensor $\mathbf{Q}$, which is work conjugate to $\mathbf{G}$ can be obtained as:

$$\mathbf{P} = \frac{\partial W_0}{\partial \mathbf{F}} = \frac{1}{2V_I} \sum_{J=1}^{3} \mathbf{f}_{IJ} \otimes \mathbf{R}_{IJ} \tag{14}$$

$$\mathbf{Q} = \frac{\partial W_0}{\partial \mathbf{G}} = \frac{1}{4V_I} \sum_{J=1}^{3} \mathbf{f}_{IJ} \otimes \mathbf{R}_{IJ} \otimes \mathbf{R}_{IJ} \tag{15}$$

where $\mathbf{f}_{IJ}$ is the generalized force associated with the generalized coordinate $\mathbf{r}_{IJ}$, which is defined as:

$$\mathbf{f}_{IJ} = \frac{\partial W}{\partial \mathbf{r}_{IJ}} \tag{16}$$

The corresponding strain energy density can also be rewritten as:

$$W_0 = W / 2V_I \tag{17}$$

Where

$$W = \sum_{J=1}^{3} V_{IJ}(\mathbf{r}_{IJ}, \mathbf{r}_{IK}, \theta_{IJK}, K \neq I, J) \tag{18}$$

denotes the total energy of the representative cell related to atom I caused by atomic interaction. V_{IJ} is the interatomic potential for carbon introduced in Section 2.
We can also define the generalized stiffness $\mathbf{K}_{IJIK}$ associated with the generalized coordinate $\mathbf{r}_{IJ}$ as:

$$\mathbf{K}_{IJIK} = \frac{\partial \mathbf{f}_{IJ}}{\partial \mathbf{r}_{IK}} = \frac{\partial^2 W}{\partial \mathbf{r}_{IJ} \partial \mathbf{r}_{IK}} \tag{19}$$

where the subscripts I, J and K in the overstriking letters, such as $\mathbf{f}$, $\mathbf{r}$, $\mathbf{R}$ and $\mathbf{K}$, denote different atoms rather than the indices of the components of tensors. Therefore summation is not implied here by the repetition of these indices.
From (14) and (15), the tangent modulus tensors can be derived as:

$$\mathbf{M}_{\mathbf{FF}} = \frac{\partial^2 W_0}{\partial \mathbf{F} \otimes \partial \mathbf{F}} = \frac{1}{2V_I} \sum_{J=1}^{3} \sum_{K=1}^{3} [\mathbf{K}_{IJIK} \underline{\otimes} (\mathbf{R}_{IJ} \otimes \mathbf{R}_{IK})] \tag{20a}$$

$$\mathbf{M}_{\mathbf{FG}} = \frac{\partial^2 W_0}{\partial \mathbf{F} \otimes \partial \mathbf{G}} = \frac{1}{4V_I} \sum_{J=1}^{3} \sum_{K=1}^{3} [\mathbf{K}_{IJIK} \underline{\otimes} (\mathbf{R}_{IJ} \otimes \mathbf{R}_{IK})] \otimes \mathbf{R}_{IK} \tag{20b}$$

$$\mathbf{M}_{\mathbf{GF}} = \frac{\partial^2 W_0}{\partial \mathbf{G} \otimes \partial \mathbf{F}} = \frac{1}{4V_I} \sum_{J=1}^{3} \sum_{K=1}^{3} [\mathbf{K}_{IJIK} \overline{\otimes} (\mathbf{R}_{IJ} \otimes \mathbf{R}_{IJ})] \otimes \mathbf{R}_{IK} \tag{20c}$$

$$\mathbf{M}_{\mathbf{GG}} = \frac{\partial^2 W_0}{\partial \mathbf{G} \otimes \partial \mathbf{G}} = \frac{1}{8V_I} \sum_{J=1}^{3} \sum_{K=1}^{3} [\mathbf{K}_{IJIK} \overline{\otimes} (\mathbf{R}_{IJ} \otimes \mathbf{R}_{IJ})] \otimes (\mathbf{R}_{IK} \otimes \mathbf{R}_{IK}) \tag{20d}$$

where $[\mathbf{A} \underline{\otimes} \mathbf{B}]_{ijkl} = A_{ik} B_{jl}$, $[\mathbf{A} \overline{\otimes} \mathbf{B}]_{ijkl} = A_{il} B_{jk}$. Compared with the results obtained by Zhang et al. (2002c), four tangent modulus tensors are presented here. This is due to the fact that second order deformation gradient tensor has been introduced here for kinematic description. Therefore, from the macroscopic point of view, we can view the SWNT as a generalized continuum with microstructure.

Just as emphasized by Cousins(1978a,b), Tadmor (1999), Zhang (2002c), Arroyo and Belytschko (2002a), since the atomic structure of carbon nanotube is not centrosymmetric, the standard Cauchy-Born rule can not be used directly since it cannot guarantee the inner equilibrium of the representative cell. An inner shift vector $\boldsymbol{\eta}$ must be introduced to achieve this goal. The inner shift vector can be obtained by minimizing the strain energy density of the unit cell with respect to $\boldsymbol{\eta}$:

$$\hat{\boldsymbol{\eta}}(\mathbf{F}, \mathbf{G}) = \arg(\min_{\boldsymbol{\eta}} W_0(\mathbf{F}, \mathbf{G}, \boldsymbol{\eta})) \Rightarrow \left. \frac{\partial W_0}{\partial \boldsymbol{\eta}} \right|_{\eta = \hat{\eta}} = \mathbf{0} \tag{21}$$

Substituting (21) into $W_0(\mathbf{F}, \mathbf{G}, \boldsymbol{\eta})$, we have:

$$\hat{W}_0(\mathbf{F}, \mathbf{G}) = W_0(\mathbf{F}, \mathbf{G}, \hat{\boldsymbol{\eta}}(\mathbf{F}, \mathbf{G})) \tag{22}$$

Then the modified tangent modulus tensors can be obtained as:

$$\hat{\mathbf{M}}_{\mathbf{FF}} = \frac{\partial^2 \hat{W}_0}{\partial \mathbf{F} \otimes \partial \mathbf{F}} = \mathbf{M}_{\boldsymbol{FF}}\big|_{\eta = \hat{\eta}} - \left[\frac{\partial^2 W_0}{\partial \mathbf{F} \otimes \partial \boldsymbol{\eta}} \left(\frac{\partial^2 W_0}{\partial \boldsymbol{\eta} \otimes \partial \boldsymbol{\eta}} \right)^{-1} \frac{\partial^2 W_0}{\partial \boldsymbol{\eta} \otimes \partial \mathbf{F}} \right] \Big|_{\eta = \hat{\eta}} \tag{23a}$$

$$\hat{\mathbf{M}}_{\mathbf{F}G} = \frac{\partial^2 \hat{W}_0}{\partial \mathbf{F} \otimes \partial \mathbf{G}} = \mathbf{M}_{\mathbf{F}G}\big|_{\eta = \hat{\eta}} - \left[\frac{\partial^2 W_0}{\partial \mathbf{F} \otimes \partial \boldsymbol{\eta}} \left(\frac{\partial^2 W_0}{\partial \boldsymbol{\eta} \otimes \partial \boldsymbol{\eta}} \right)^{-1} \frac{\partial^2 W_0}{\partial \boldsymbol{\eta} \otimes \partial \mathbf{G}} \right] \Big|_{\eta = \hat{\eta}} \tag{23b}$$

$$\hat{\mathbf{M}}_{\mathbf{GF}} = \frac{\partial^2 \hat{W}_0}{\partial \mathbf{G} \otimes \partial \mathbf{F}} = \mathbf{M}_{\mathbf{GF}}\big|_{\eta = \hat{\eta}} - \left[\frac{\partial^2 W_0}{\partial \mathbf{G} \otimes \partial \boldsymbol{\eta}} \left(\frac{\partial^2 W_0}{\partial \boldsymbol{\eta} \otimes \partial \boldsymbol{\eta}} \right)^{-1} \frac{\partial^2 W_0}{\partial \boldsymbol{\eta} \otimes \partial \mathbf{F}} \right] \Big|_{\eta = \hat{\eta}} \tag{23c}$$

$$\hat{\mathbf{M}}_{GG} = \frac{\partial^2 \hat{W}_0}{\partial \mathbf{G} \otimes \partial \mathbf{G}} = \mathbf{M}_{GG}\big|_{\eta = \hat{\eta}} - \left[\frac{\partial^2 W_0}{\partial \mathbf{G} \otimes \partial \boldsymbol{\eta}} \left(\frac{\partial^2 W_0}{\partial \boldsymbol{\eta} \otimes \partial \boldsymbol{\eta}} \right)^{-1} \frac{\partial^2 W_0}{\partial \boldsymbol{\eta} \otimes \partial \mathbf{G}} \right] \Big|_{\eta = \hat{\eta}} \tag{23d}$$

Where

$$\mathbf{M}_{FF}\big|_{\eta = \hat{\eta}} = \frac{1}{2V_I} \sum_{J=1}^{3} \sum_{K=1}^{3} [\hat{\mathbf{K}}_{IJIK} \underline{\otimes} ((\mathbf{R}_{IJ} + \hat{\boldsymbol{\eta}}) \otimes (\mathbf{R}_{IJ} + \hat{\boldsymbol{\eta}}))] \tag{24a}$$

$$\mathbf{M_{FG}}\big|_{\boldsymbol{\eta}=\hat{\boldsymbol{\eta}}} = \frac{1}{4V_I}\sum_{J=1}^{3}\sum_{K=1}^{3}[\hat{\mathbf{K}}_{IJIK}\underline{\otimes}((\mathbf{R}_{IJ}+\hat{\boldsymbol{\eta}})\otimes(\mathbf{R}_{IK}+\hat{\boldsymbol{\eta}})]\otimes(\mathbf{R}_{IK}+\hat{\boldsymbol{\eta}}\blacksquare \tag{24b}$$

$$\mathbf{M_{GF}}\big|_{\eta=\hat{\eta}} = \frac{1}{4V_I}\sum_{J=1}^{3}\sum_{K=1}^{3}[\hat{\mathbf{K}}_{IJIK}\overline{\otimes}((\mathbf{R}_{IJ}+\hat{\boldsymbol{\eta}})\otimes(\mathbf{R}_{IJ}+\hat{\boldsymbol{\eta}}))]\otimes(\mathbf{R}_{IK}+\hat{\boldsymbol{\eta}}) \tag{24c}$$

$$\mathbf{M_{GG}}\big|_{\eta=\hat{\eta}} = \frac{1}{8V_I}\sum_{J=1}^{3}\sum_{K=1}^{3}[\hat{\mathbf{K}}_{IJIK}\overline{\otimes}((\mathbf{R}_{IJ}+\hat{\boldsymbol{\eta}})\otimes(\mathbf{R}_{IJ}+\hat{\boldsymbol{\eta}}))]\otimes((\mathbf{R}_{IK}+\hat{\boldsymbol{\eta}})\otimes(\mathbf{R}_{IK}+\hat{\boldsymbol{\eta}})) \tag{24d}$$

$$\hat{\mathbf{K}}_{IJIK} = \left.\frac{\partial^2 W}{\partial \mathbf{r}_{IJ}\otimes\partial \mathbf{r}_{IJ}}\right|_{\eta=\hat{\eta}\ ,\ \mathbf{r}_{IJ}=\hat{\mathbf{r}}_{IJ}} \tag{25}$$

$$\hat{\mathbf{r}}_{IJ} = \mathbf{F}\bullet(\mathbf{R}_{IJ}+\hat{\boldsymbol{\eta}}) + \mathbf{G}:[(\mathbf{R}_{IJ}+\hat{\boldsymbol{\eta}})\otimes(\mathbf{R}_{IJ}+\hat{\boldsymbol{\eta}})]/2 \tag{26}$$

$$\begin{aligned}\frac{\partial^2 W_0}{\partial \mathbf{F}\otimes\partial\boldsymbol{\eta}}\Big|_{\eta=\hat{\eta}} = \frac{1}{2V_I}\sum_{J=1}^{3}[\sum_{K=1}^{3}((\hat{\mathbf{K}}_{IJIK}\bullet\mathbf{F})\dot{\otimes}(\mathbf{R}_{IJ}+\hat{\boldsymbol{\eta}}) \\ +\dot{sym}(\hat{\mathbf{K}}_{IJIK}\bullet\mathbf{G}\bullet((\mathbf{R}_{IK}+\hat{\boldsymbol{\eta}})\otimes(\mathbf{R}_{IJ}+\hat{\boldsymbol{\eta}}))))+\hat{\mathbf{f}}_{IJ}\otimes{}^2\mathbf{1}]\end{aligned} \tag{27}$$

$$\frac{\partial W_0}{\partial \boldsymbol{\eta}}\Big|_{\eta=\hat{\eta}} = \frac{1}{2V_I}\sum_{J=1}^{3}\hat{\mathbf{f}}_{IJ}\bullet[\mathbf{F}+\dot{sym}(\mathbf{G}\bullet(\mathbf{R}_{IJ}+\hat{\boldsymbol{\eta}}))] \tag{28}$$

$$\begin{aligned}\frac{\partial^2 W_0}{\partial \boldsymbol{\eta}\otimes\partial\mathbf{F}}\Big|_{\eta=\hat{\eta}} = \frac{1}{2V_I}\sum_{J=1}^{3}[\sum_{K=1}^{3}((\mathbf{F}+\dot{sym}(\mathbf{G}\bullet(\mathbf{R}_{IJ}+\hat{\boldsymbol{\eta}})))^{\mathbf{T}} \\ \bullet(\hat{\mathbf{K}}_{IJIK}\otimes(\mathbf{R}_{IK}+\hat{\boldsymbol{\eta}})))+\hat{\mathbf{f}}_{IJ}\dot{\otimes}{}^2\mathbf{1}]\end{aligned} \tag{29}$$

$$\begin{aligned}\frac{\partial^2 W_0}{\partial \boldsymbol{\eta}\otimes\partial\boldsymbol{\eta}}\Big|_{\eta=\hat{\eta}} = \frac{1}{2V_I}\sum_{J=1}^{3}[\sum_{K=1}^{3}(\mathbf{F}+\dot{sym}(\mathbf{G}\bullet(\mathbf{R}_{IJ}+\hat{\boldsymbol{\eta}})))^{\mathbf{T}}\bullet\hat{\mathbf{K}}_{IJIK} \\ \bullet(\mathbf{F}+\dot{sym}(\mathbf{G}\bullet(\mathbf{R}_{IK}+\hat{\boldsymbol{\eta}}))))+\hat{\mathbf{f}}_{IJ}\bullet\dot{sym}\,\mathbf{G}]\end{aligned} \tag{30}$$

$$\begin{aligned}\frac{\partial^2 W_0}{\partial \mathbf{G}\otimes\partial\boldsymbol{\eta}}\Big|_{\eta=\hat{\eta}} = \frac{1}{4V_I}\sum_{J=1}^{3}[\sum_{K=1}^{3}(\dot{sym}(\hat{\mathbf{K}}_{IJIK}\bullet\mathbf{G}\bullet((\mathbf{R}_{IK}+\hat{\boldsymbol{\eta}})\otimes(\mathbf{R}_{IJ}+\hat{\boldsymbol{\eta}})\otimes(\mathbf{R}_{IJ}+\hat{\boldsymbol{\eta}})))) \\ +(\hat{\mathbf{K}}_{IJIK}\bullet\mathbf{F})\dot{\otimes}(\mathbf{R}_{IK}+\hat{\boldsymbol{\eta}})\dot{\otimes}(\mathbf{R}_{IK}+\hat{\boldsymbol{\eta}}))+(\hat{\mathbf{f}}_{IJ}\overline{\otimes}(\mathbf{R}_{IJ}+\hat{\boldsymbol{\eta}})\overline{\otimes}{}^2\mathbf{1}) \\ +(\hat{\mathbf{f}}_{IJ}\otimes(\mathbf{R}_{IJ}+\hat{\boldsymbol{\eta}})\otimes{}^2\mathbf{1})]\end{aligned} \tag{31}$$

$$\frac{\partial^2 W_0}{\partial \boldsymbol{\eta} \otimes \partial \mathbf{G}}\Big|_{\eta=\hat{\eta}} = \frac{1}{2V_I}\sum_{J=1}^{3}[\sum_{K=1}^{3}(\frac{1}{2}((\mathbf{F} + \overset{\bullet}{sym}(\mathbf{G} \bullet (\mathbf{R}_{IJ} + \hat{\boldsymbol{\eta}})))^{\mathbf{T}} \bullet (\hat{\mathbf{K}}_{IJIK} \otimes (\mathbf{R}_{IK} + \hat{\boldsymbol{\eta}}) \otimes (\mathbf{R}_{IK} + \hat{\boldsymbol{\eta}})))) + \overset{\bullet}{sym}(\hat{\mathbf{f}}_{IJ} \otimes {}^2\mathbf{1} \otimes (\mathbf{R}_{IJ} + \hat{\boldsymbol{\eta}}))] \tag{32}$$

where ${}^2\mathbf{1}$ is the second order identity tensor. The symbols used in the above expressions are defined as:

$$(\overset{\bullet}{sym}[\mathbf{A} \bullet \mathbf{B} \bullet (\mathbf{c} \otimes \mathbf{d})])_{ijk} = (A_{ip}B_{pkn}c_n d_j + A_{ip}B_{pqk}c_q d_j)/2 \tag{33}$$

$$(\mathbf{A} \overset{\bullet}{\otimes} \mathbf{b})_{ijk} = A_{ik}b_j \tag{34}$$

$$[\overset{\bullet}{sym}(\mathbf{B} \bullet \mathbf{b})]_{ij} = (B_{ijr}b_r + B_{irj}b_r)/2 \tag{35}$$

$$(\mathbf{a} \overset{\bullet}{\otimes} \mathbf{A})_{ijk} = a_j A_{ik} \tag{36}$$

$$(\overset{\bullet}{sym}\mathbf{G})_{ijk} = (G_{ijk} + G_{ikj})/2 \tag{37}$$

$$[(\mathbf{a} \overline{\otimes} \mathbf{b}) \overline{\otimes} \mathbf{A}]_{ijkl} = a_i b_k A_{jl} \tag{38}$$

$$(\overset{\bullet}{sym}[\mathbf{A} \bullet \mathbf{B} \bullet (\mathbf{c} \otimes \mathbf{d} \otimes \mathbf{d})])_{ijkl} = (A_{ip}B_{plr}c_r d_j d_k + A_{ip}B_{pql}c_q d_j d_k)/2 \tag{39}$$

$$(\mathbf{A} \overset{\bullet}{\otimes} \mathbf{c} \overset{\bullet}{\otimes} \mathbf{c})_{ijkl} = A_{il}c_j c_k \tag{40}$$

$$(\overset{\bullet}{sym}(\mathbf{a} \otimes \mathbf{A} \otimes \mathbf{b}))_{ijkl} = (a_j A_{ik}b_l + a_j A_{il}b_k)/2 \tag{41}$$

5. Mechanical properties of SWCNTs

It is usually thought that SWCNTs can be formed by rolling a graphite sheet into a hollow cylinder. To predict mechanical properties of SWCNTs, a planar graphite sheet in equilibrium energy state is here defined as the undeformed configuration, and the current configuration of the nanotube can be seen as deformed from the initial configuration by the following mapping:

$$\begin{aligned} x_1 &= \alpha_1 X_1 \\ x_2 &= \alpha_2 R_0 \sin(\frac{X_2}{R_0} + \kappa\alpha_1 X_1) \\ x_3 &= \alpha_2 R_0 (\cos(\frac{X_2}{R_0} + \kappa\alpha_1 X_1) - 1) \end{aligned} \tag{42}$$

where X_i, $i=1,2$ is Lagrange coordinate associated with the undeformed configuration (here is a graphite sheet) and x_i, $i=1,2,3$ is Eulerian coordinate associated with the deformed configuration. R is the radius of the modeled SWCNT, which is described by a pair of parameters (n,m). The radius R can be evaluated by $R=a\sqrt{m^2+mn+n^2}/2\pi$ with $a=a_0\sqrt{3}$, where a_0 is the equilibrium bond length of the atoms in the graphite sheet. κ represents the rotation angle per unit length, and parameters α_1 and α_2 control the uniform axial and circumferential stretch deformation, respectively.

5.1 The energy per atom for graphene sheet and SWCNTs

First, based on the present model, the energy per atom of the graphite sheet is calculated and the value of -1.1801 $Kg\,nm^2/s^2$ is obtained. It can be found that the present value agrees well with that of -7.3756 eV ($1eV=1.6\times10^{-19}\ Nm$) given by Robertson et al. (1992) with the use of the same interatomic potential.

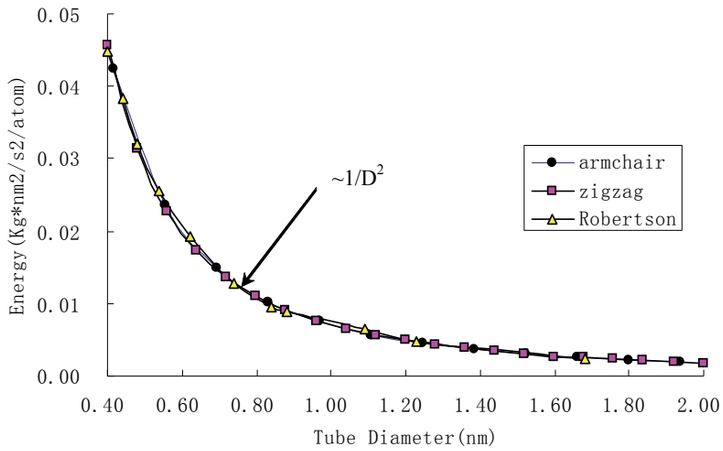

Fig. 4. The energy (relative to graphite) per atom versus tube diameter

The energy per atom as the function of diameters for armchair and zigzag SWNTs relative to that of the graphene sheet is shown in Figure 4. The trend is almost the same for both armchair and zigzag SWNTs. The energy per atom decreases with increase of the tube diameter with $E(D)-E(\infty)=O(1/D^2)$, where $E(\infty)$ represents the energy per atom for graphite sheet.

For larger tube diameter, the energy per atom approaches that of graphite. On the whole, it can be shown that the energy per atom depends obviously on tube diameters, but does not depend on tube chirality. For comparison, the results obtained by Robertson et al. (1992) with the use of both empirical potential and first-principle method based on the same interatomic potential are also shown in Figure 4. It can be found the present results are not only in good agreement with Robertson's results, but also with those obtained by Jiang et al. (2003) based on incorporating the interatomic potential (Tersoff-Brenner potential) into the continuum analysis.

Figure 5 shows the energy per atom for different chiral SWCNTs ((2n, n), (3n, n), (4n, n), (5n, n) and (8n, n)) as a function of tube radius relative to that of the graphene sheet. As is expected, the energy per atom of chiral SWCNTs decreases with increasing tube radius and

the limit value of this quantity is -7.3756 eV when the radius of tube is large. From Figure 5, it can be clearly found again that the strain energy per atom depends only on the radius of the tube and is independent of the chirality of SWCNTs, which is similar to armchair and zigzag SWCNTs.

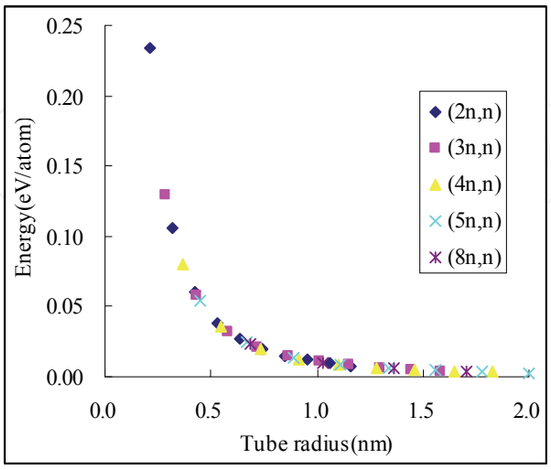

Fig. 5. The strain energy relative to graphite (eV/atom) as a function of tube radius.

5.2 Young's modulus and Poisson ratio for graphene sheet and SWCNTs

As shown by Zhang et al. (2002c), the Young's modulus and the Poisson's ratio of planar graphite can be defined from $\hat{\mathbf{M}}_{FF}$ by the following expressions:

$$E = (\hat{\mathbf{M}}_{FF})_{1111} - \frac{(\hat{\mathbf{M}}_{FF})_{1122}^2}{(\hat{\mathbf{M}}_{FF})_{2222}} \tag{43}$$

$$v = \frac{(\hat{\mathbf{M}}_{FF})_{1122}}{(\hat{\mathbf{M}}_{FF})_{1111}} \tag{44}$$

For SWCNTs, we also use the above expressions to estimate their mechanical properties along the axial direction although the corresponding elasticity tensors are no longer isotropic as in planar graphite case. Note that all calculations performed here are based on the Cartesian coordinate system and the Young's modulus E is obtained by dividing the thickness of the wall of SWNT, which is often taken as 0.334nm in the literature.

As for the graphite, the resulting Young's modulus is 0.69TP (see the dashed line in Figure 6a), which agrees well with that suggested by Zhang et al (2002c) and Arroyo and Belytschko (2004b) based on the same interatomic potential (represents by the horizontal solid line in Figure 6a). The Poisson's ratio predicted by the present approach is 0.4295 (see the dashed line shown in Figure 6c), which is also very close to the value of 0.4123 given by Arroyo and Belytschko (2004b) using the same interatomic potential.

As for armchair and zigzag SWCNTs, Figure 6a displays the variations of the Young's modulus with different diameters and chiralities. It can be observed that the trend is similar for both armchair and zigzag SWNTs and the influence of nanotube chirality is not significant. For smaller tubes whose diameters are less than 1.3 nm, the Young's modulus strongly depends on the tube diameter. However, for tubes diameters larger than 1.3 nm, the

dependence becomes very weak. As a whole, it can be seen that for both armchair and zigzag SWNTs the Young's modulus increases with increase of tube diameter and a plateau is reached when the diameter is large, which corresponds to the modulus of graphite predicted by the present method. The existing non-orthogonal tight binding results given by Hernández et al.(1998), lattice-dynamics results given by Popov et al. (2000) and the exponential Cauchy-Born rule based results given by Arroyo and Belytschko (2002b) are also shown in Figure 6a for comparison. Comparing with the results given by Hernández et al. (1998) and Popov et al. (2000), it can be seen that although their data are larger than the corresponding ones of the present model, the general tendencies predicted by different methods are in good agreement. From the trend to view, the present predicted trend is also in reasonable agreement with that given by Robertson et al. (1992), Arroyo and Belytschko (2002b), Chang and Gao (2003) and Jiang et al. (2003). As for the differences between the values of different methods, it may be due to the fact that different parameters and atomic potential are used in different theories or algorithms (Chang and Gao, 2003). For example, Yakobson's (1996) result of surface Young's modulus of carbon nanotube based on molecular dynamics simulation with Tersoff-Brenner potential is about 0.36TPa nm, while Overney's (1993) result based on Keating potential is about 0.51 TP nm. Recent *ab initio* calculations by Sánchez-Portal et al.(1999) and Van Lier et al. (2000) showed that Young's modulus of SWNTs may vary from 0.33 to 0.37TPa nm and from 0.24 to 0.40 TPa nm, respectively. Furthermore, it can be found that our computational results agree well with that given by Arroyo and Belytschko (2002b) with their exponential Cauchy-Born rule. They are also in reasonable agreement with the experimental results of 0.8 ± 0.4 TP given by Salveta et al. (1999).

Figure 6b depicts the size-dependent Young's moduli of different chiral SWCNTs ((2n, n), (3n, n), (4n, n), (5n, n) and (8n, n)). It can be seen that Young's moduli for different chiral SWCNTs increase with increasing tube radius and approach the limit value of graphite when the tube radius is large. For a given tube radius, the effect of tube chirality can almost be ignored. The Young's modulus of different chiral SWCNTs are consistent in trends with those for armchair and zigzag SWCNTs. For chiral SWCNTs, the trends of the present results are also in accordance with those given by other methods, including lattice dynamics (Popov et al., 2000) and the analytical molecular mechanics approach (Chang & Gao, 2003) .

From Figure 6c, the effect of tube diameter on the Poisson's ratio is also clearly observed. It can be seen that, for both armchair and zigzag SWNTs, the Poisson's ratio is very sensitive to the tube diameters especially when the diameter is less than 1.3 nm. The Poisson's ratio of armchair nanotube decreases with increasing tube diameter but the situation is opposite for that of the zigzag one. However, as the tube diameters are larger than 1.3 nm, the Poisson's ratio of both armchair and zigzag SWNTs reach a limit value i.e. the Poisson's ratio of the planar graphite. For comparison, the corresponding results suggested by Popov et al. (2000) are also shown in Figure 6c. It can be observed that the tendencies are very similar between the results given by Popov et al. (2000) and the present method although the values are different. Moreover, it is worth noting although many investigations on the Poisson's ratio of SWNTs have been conducted, there is no unique opinion that is widely accepted. For instance, Goze et al. (1999) showed that the Poisson's ratio of (10,0), (20,0), (10,0) and (20,0) tubes are 0.275, 0.270, 0.247 and 0.256, respectively. Based on a molecular mechanics approach, Chang and Gao (2003) suggested that the Poisson's ratio for armchair and zigzag SWNTs will decrease with increase of tube diameters from 0.19 to 0.16, and 0.26 to 0.16, respectively. In recent *ab initio* studies of Van Lier et al. (2000), even negative Poisson's ratio is reported.

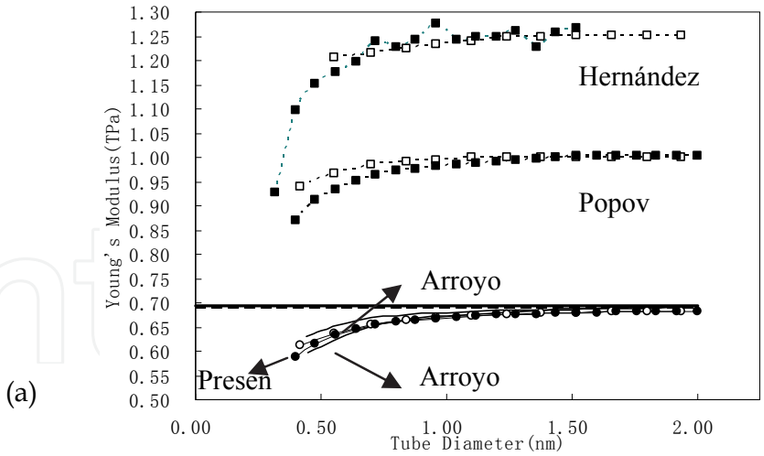

(a)

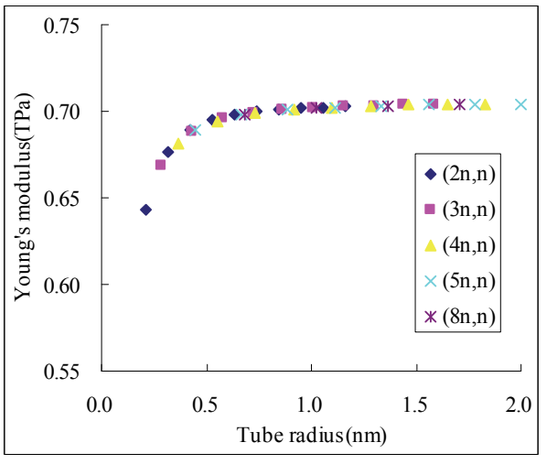

(b)

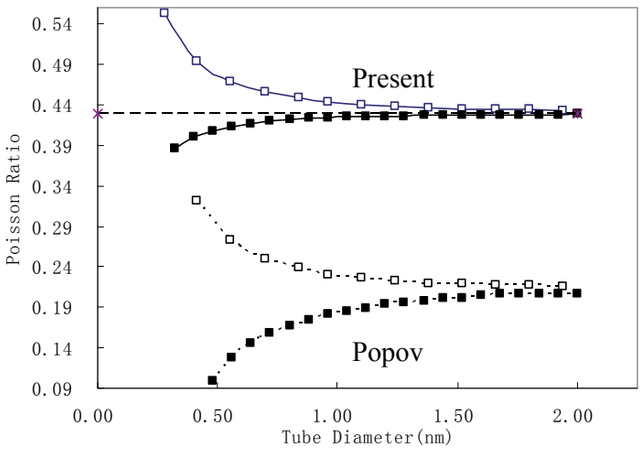

(c)

Fig. 6. Comparison between the results obtained with different methods (a) Young's modulus and (b) Young's moduli of chiral SWCNTs versus tube radius. (c)Poisson's ratio. Open symbols denote armchair, solid symbols denote zigzag. Dashed horizontal line denotes the results of graphite obtained with the present approach and the solid horizontal line denotes the results of graphite obtained by Arroyo and Belytschko (2004b) with exponential mapping, respectively.

It also can be seen from Figure 6c that the obtained Poisson's ratio is a little bit high when tube diameter is less than 0.3nm. It may be ascribed to the fact that when tube diameter is less than 0.3nm, because of the higher value of curvature, higher order (≥ 2) deformation gradient tensor should be taken into account in order to describe the deformation of the atomic bonds more accurately. Another possible explanation is that for such small values of diameter, more accurate interatomic potential should be used in this extreme case.

5.3 Shear modulus for SWCNTs

As for the shear moduli of SWCNTs, to the best of our knowledge, only few works studied this mechanical property systematically since it is difficult to measure them with experiment techniques. Most of these works focus only on the armchair and zigzag SWCNTs.(Popov et al., 2000; Li & Chou, 2003) Thus, the shear moduli of achiral (i.e., armchair and zigzag) SWCNTs are firstly investigated and compared with the existing results (Li & Chou, 2003) for validation of the present model. Then the shear modulus of SWCNTs with different chiralities including (2n, n), (3n, n), (4n, n), (5n, n) and (8n, n) are studied systematically. For determining the shear modulus of SWCNT, it is essential to simulate its pure torsion deformation which can be implemented by incrementally controlling κ but relaxing inner displacement $\boldsymbol{\eta}$, parameters α_1 and α_2 in Equation (42). The shear modulus of SWCNTs can be obtained by the U (strain energy density) and κ (twist angle per unit length). Similar to Young's modulus, shear modulus is defined with respect to the initial stress free state.

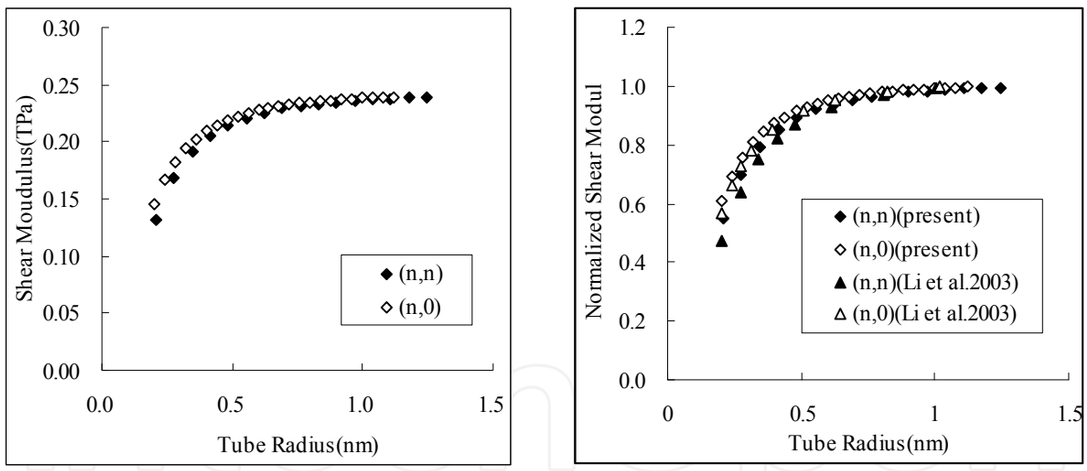

(a) (b)

Fig. 7. (a) Shear moduli of armchair and zigzag SWCNTs versus tube radius, (b) Effect of tube radius on normalized shear moduli of armchair and zigzag SWCNTs.

Figure 7a shows the variations of the shear modulus of achiral SWCNTs with respect to the tube radius. It can be found that shear modulus of armchair and zigzag SWCNTs increase with increasing tube radius and approach the limit value 0.24 TPa when the tube radius is large. It is also observed that, similar to the results given by Li & Chou (2003) and Xiao et al. (2005), the present predicted shear moduli of armchair and zigzag SWCNTs hold similar size-dependent trends and the chirality-dependence of shear moduli is not significant.

Figure 7b shows the normalized shear moduli obtained with different methods. The normalization is achieved by using the values of 0.24 TPa and 0.48 TPa which are the limiting values of graphite sheet obtained by the present approach and molecular structural mechanics (Li & Chou, 2003), respectively. Although there is a discrepancy in limit values, it can be found that the size effect obtained by the present study is in good agreement with that of Li and Chou (2003). The difference among the limit values may be attributed to the different atomistic potential and/or force field parameters used in the computation model.
The size-dependent shear modulus of different chiralities SWCNTs are displayed in Figure 8. It is observed that, similar to achiral SWCNTs, the shear moduli of chiral SWCNTs increase with increasing tube radius and a limit value of 0.24 TPa is approaching when the tube radius (also n) is large. For (2n, n) SWCNT, the maximum difference of shear modulus is up to 42%. The dependence of tube chirality is not obvious for chiral SWCNTs. With reference to Figure 7a and Figure 8, it can be found that, at small radius (<1nm), the shear modulus of SWCNTs are sensitive to the tube radius, while at larger radius (>1nm), the size and chirality dependency can be ignored.

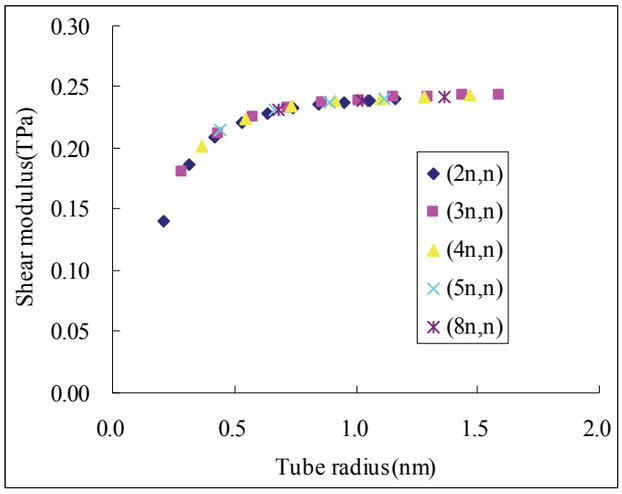

Fig. 8. Shear moduli of chiral SWCNTs versus tube radius.

5.4 Bending stiffness for graphene sheet and SWCNTs

In present study, the so-called bending stiffness for graphene sheet refers to the resistance of a flat graphite sheet or the curved wall of CNT with respect to the infinitesimal local bending deformation. The bending stiffness for SWCNTs refers to the bending resistance of the cylindrical tube formed by rolling up graphite sheet with respect to the infinitesimal global bending deformation (see Figure 9 for reference). It should be pointed out that for the first definition, the bending stiffness is an intrinsic material property solely determined by the atomistic structure of the mono-layer crystalline membrane. The second definition, however, is a *structural property* which is determined not only by the bending stiffness of the single atom layer crystalline membrane, but also by the geometry dimensions, such as the diameter of the tube. Unfortunately, these two issues are not well addressed in the past literatures (Kudin et at., 2001; Enomoto et al., 2006).
Based on the higher order Cauchy-Born rule and Equation (42), the strain energy per atom (energy relative to a planar graphite sheet) as a function of the radius of bending curvature can

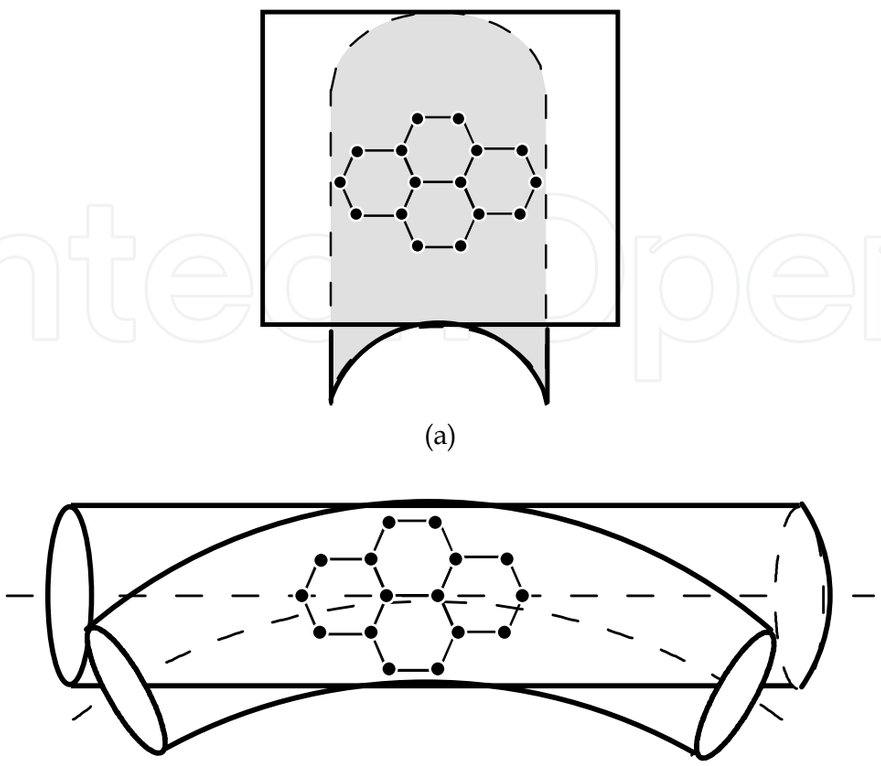

(a)

(b)

Fig. 9. (a) Bending of a flat graphite sheet; (b) Bending of a single-walled carbon nanotube

be obtained. By fitting the data of the strain energy and the bending curvature radii with respect to the equation $U = D_{membrane} / 2R_0^2$, one can obtain that the bending stiffness $D_{membrane}$ of the graphite sheet is 2.38 eVÅ²/atom, which is almost independent of its rolling direction. This indicates that the flat graphite sheet is nearly isotropic with regard to bending. The current result agrees well with the effective bending stiffness of graphite sheet 2.20 eVÅ²/atom reported by Arroyo and Belytschko (2004a) with membrane theory and the same interatomic potential under the condition of infinitesimal bending. It is also in good agreement with the result of 2.32 eVÅ²/atom obtained by Robertson et al. (1992) with atomic simulations.

To explore the effective bending stiffness of carbon nanotube based on the higher order Cauchy-Born rule, the following map is used to describe the pure bending deformation of the tube

$$\begin{aligned} x_1 &= \rho \sin(X_1/\rho) - R\sin(X_2/R)\sin\alpha \\ x_2 &= \rho \sin^2(X_1/\rho)/2 + R\sin(X_2/R)\cos\alpha \\ x_3 &= R\cos(X_2/R) \qquad (\alpha = \arctan(X_1/\rho)) \end{aligned} \tag{45}$$

where R is the radius of the modeled SWCNT and ρ is the radius of curvature of the bending tube (curvature of the neutral axis). With the use of this mapping and taking the inner-displacement relaxation into consideration, the strain energy of the bending tube can be computed.

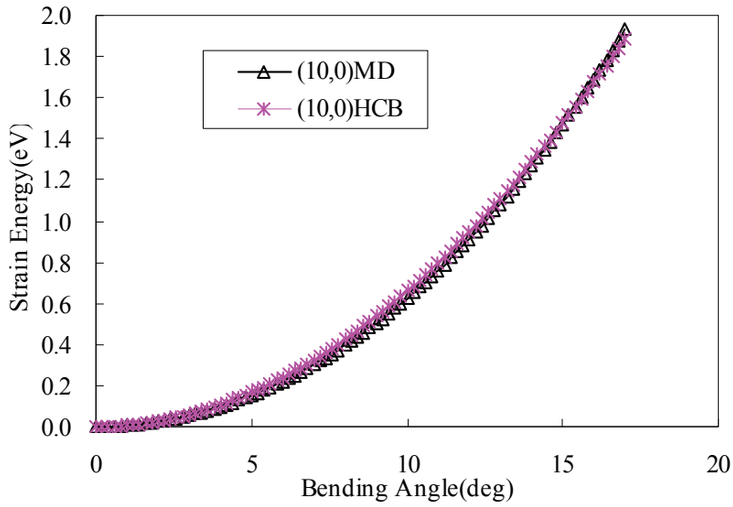

Fig. 10. Comparison of the strain energy of (10,0) SWCNT as a function of the bending angle for HCB(—✳—) and MD(—△—) simulation. Herein and after, HCB refers to the continuum theory based on a higher-order Cauchy-Born rule and MD refers to molecular dynamics

Figure 10 show the bending strain energy of zigzag (10,0) SWCNT as a function of bending angle. Here the bending strain energy is defined as the difference between the energy of the deformed tube and that of its straight status. It can be found that the present results obtained with much less computational effort are in good agreement with those of MD simulations.

where L denotes the length of the tube. It can be seen clearly from Equation (46) that the effective bending stiffness of CNTs can be defined as the second derivative of the elastic energy per unit length with respect to the curvature of the neutral axis under pure bending (i.e. constant curvature). Its dimension is $eV \cdot nm$. Figure 11 shows the bending stiffness of different chiral SWCNTs as a function of the tube radius. It can be found that the bending stiffness is almost independent on the chirality of SWCNTs and increases with the increasing of tube radius. Furthermore, using a polynomial fitting procedure, we can approximate the bending stiffness over the considered range of tube radii by the following analytical expression

Once the bending strain energy U is known, the effective bending stiffness of carbon nanotube can be obtained by numerical differentiation based on the following formula

$$U = D_{tube} L \kappa^2 / 2 \tag{46}$$

Just like the derivation of the bending stiffness of the flat graphite sheet, here no representative thickness of the tube is required to obtain the effective bending stiffness of CNTs.

$$\begin{aligned} D_{tube}(eV \cdot nm) = 5583.956(eV/nm^2)R^3(nm^3) + 9.225(eV/nm)R^2(nm^2) \\ - 32.418(eV)R(nm) + 1.517(eV \cdot nm) \end{aligned} \tag{47}$$

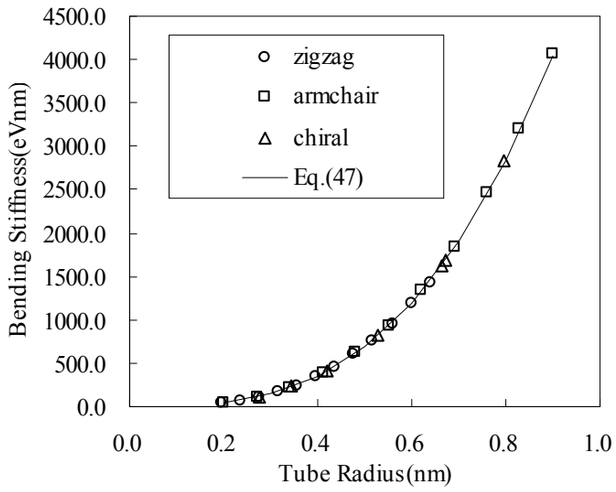

Fig. 11. Variation of bending stiffness with tube radius for different chiral SWCNTs

6. Conclusion

In this charpter, a higher order Cauchy-Born rule has been constructed for studying mechanical properties of graphene sheet and carbon nanotubes. In the present model, by including the second order deformation gradient tensor in the kinematic description, we can alleviate the limitation of the standard Cauchy-Born rule for the modeling of nanoscale crystalline films with less computational efforts. Based on the established relationship between the atomic potential and the macroscopic continuum strain energy, analytical expressions for the tangent modulus tensors are derived. From these expressions, the hyper-elastic constitutive law for this generalized continuum can be obtained.

With the use of this constitutive model and the Tersoff-Brenner atomic potential for carbon, the size and chirality dependent mechanical properties (including strain energy, Young's modulus, Poisson's ratio, shear modulus, bending stiffness) of graphene sheet and carbon nanotube are predicted systematically. The present investigation shows that except for Poisson's ratio other mechanical properties (such as Young's modulus, shear modulus, bending stiffness and so on) for graphene sheet and SWCNTs are size-dependent and their chirality-dependence is not significant. With increasing of tube radius, Young's modulus and shear modulus of SWCNTs increase and converge to the corresponding limit values of graphene sheet. As for Poisson's ratio, it can be found that it is very sensitive to the radius and the chirality of SWCNTs when the tube diameter is less than 1.3 nm. The present results agree well with those obtained by other experimental, atomic modeling and continuum concept based studies.

Besides, the present work also discusses some basic problems on the study of the bending stiffness of CNTs. It is pointed out that the bending stiffness of a flat graphite sheet and that of CNTs are two different concepts. The former is an intrinsic material property while the later is a structural one. Since the smeared-out model of CNTs is a generalized continuum with microstructure, the effective bending stiffness of it should be regarded as an independent structural rigidity parameter which can not be determined simply by employing the classic formula in beam theory. It is hoped that the above findings may be helpful to clarify some obscure issues on the study of the mechanical properties of CNTs both theoretically and experimentally.

It should be pointed out that the present method is not limited to a specific interatomic potential and the study of SWCNTs. It can also be applied to calculate the mechanical response of MWCNTs. The proposed model can be further applied to other nano-film materials. The key point is to view them as generalized continuum with microstructures.

7. Acknowledgment

This work was supported by the National Natural Science Foundation of China (10802076), the Nature Science Foundation of Zhejiang province (Y6090543), China Postdoctoral Science Foundation (20100470072) and the Scientific Research Foundation of Zhejiang Ocean University.

8. References

Arroyo, M. & Belytschko, T. (2002). An atomistic-based finite deformation membrane for single layer crystalline films. Journal of the Mechanics and Physics of Solids, 50, 1941-1977.

Arroyo, M. & Belytschko, T. (2004a). Finite element methods for the non-linear mechanics of crystalline sheets and nanotubes. International Journal for Numerical Methods in Engineering, 59, 419-456.

Arroyo, M. & Belytschko, T. (2004b). Finite crystal elasticity of carbon nanotubes based on the exponential Cauchy-Born rule. Physical Review B, 69, 115415-1-11.

Bhattacharya, K. & James, R.D. (1999). A theory of thin films with applications to microstructures. Journal of the Mechanics and Physics of Solids, 47, 465-502.

Brenner, D.W. (1990). Empirical potential for hydrocarbons for use in simulation the chemical vapor deposition of diamond films. Physical Review B, 42, 9458-9471.

Chang, T.C. & Gao, H.J. (2003) Size-dependent elastic properties of a single-walled carbon nanotube via a molecular mechanics model. Journal of the Mechanics and Physics of Solids, 51, 1059-1074.

Cousins, C.S.G. (1978a). Inner elasticity. Journal of Physics C: Solid State Physics, 11, 4867-4879.

Cousins, C.S.G. (1978b). The symmetry of inner elastic constants. Journal of Physics C: Solid State Physics, 11, 4881-4900.

Enomoto, K.; Kitakata, S.; Yasuhara, T.; Ohtake, N.; Kuzumaki, T. & Mitsuda, Y. (2006) Measurement of Young's modulus of carbon nanotubes by nanoprobe manipulation in a transmission electron microscope. Applied Physics Letters, 88, 153115-1-3.

Garstein, Y.N.; Zakhidov, A.A. & Baughman, R.H. (2003) Mechanical and electromechanical coupling in carbon nanotube distortions. Physical Review B, 68, 115415.

Govindjee, S. & Sackman, J.L. (1999). On the use of continuum mechanics to estimate the properties of nanotubes. Solid State Communication, 110, 227-230.

Goze, C.; Vaccarini, L.; Henrard, L.; Bernier, P.; Hernández, E. & Rubio, A. (1999). Elastic and mechanical properties of carbon nanotubes. Synthetic Metals, 103, 2500-2501.

Guo, X.; Wang, J.B. & Zhang, H.W. (2006) Mechanical properties of single-walled carbon nanotubes based on higher order Cauchy-Born rule. International Journal of Solids and Structures, 43(5), 1276-1290.

He, X.Q.; Kitipornchai, S. & Liew, K.M. (2005a). Buckling analysis of multi-walled carbon nanotubes: a continuum model accounting for van der Waals interaction. Journal of the Mechanics and Physics of Solids, 53, 303-326.

He, X.Q.; Kitipornchai, S.; Wang, C.M. & Liew K.M. (2005b). Modeling of van der Waals force for infinitesimal deformation of multi-walled carbon nanotubes treated as cylindrical shells. International Journal of Solids and Structures, 42, 6032-6047.

Hernández, E.; Goze, C.; Bernier, P. & Rubio, A. (1998). Elastic properties of C and BxCyNz composite nanotubes. Physical Review Letters, 80, 4502-4505

Iijima, S. (1991). Helical microtubules of graphitic carbon. Nature, 354, 56-58.

Iijima, S. & Ichlhashi T. (1993). Single-shell carbon nanotubes of 1-nm diameter. Nature, 363, 603-605.

Iijima, S.; Brabec, C.; Maiti, A. & Bernholc, J. (1996). Structural flexibility of carbon nanotubes. Journal of Chemical Physics, 104, 2089-2092.

Jiang, H.; Zhang, P.; Liu, B.; Huang, Y.; Geubelle, P.H.; Gao, H. & Hwang K.C. (2003). The effect of nanotube radius on the constitutive model for carbon nanotubes. Computational Materials Science, 28, 429-442.

Krishnan, A.; Dujardin, E.; Ebbesen, T.W.; Yianilos, P.N. & Treacy, M.M.J. (1998). Young's modulus of single-walled nanotubes. Physical Review B, 58, 14013-14019.

Kudin, D.; Scuseria, G. & Yakobson, B. (2001). C2, BN, and C nanoshell elasticity from ab initio computations. Physical Review B, 64, 235406

Leamy, M.J.; Chung, P.W. & Namburu, R. (2003). On an exact mapping and a higher-order Born rule for use in analyzing graphene carbon nanotubes. Proceedings of the 11th Annual ARL-USMA Technical Symposium, November 5.

Li, C.Y. & Chou, T.W. (2003). A structural mechanics approach for analysis of carbon nanotubes. International Journal of Solids and Structures, 40, 2487-2499.

Liang, H.Y. & Upmanyu, M. (2006) Axial-strain-induced torsion in single-walled carbon nanotubes. Physical Review Letters, 96, 165501.

Mu, W.H.; Li, M.; Wang, W. & Ou-Yang, Z.C. (2009) Study of axial strain-induced torsion of single-wall carbon nanotubes using the 2D continuum anharmonic anisotropic elastic model. New Journal of Physics, 11, 113049.

Odega, G.M.; Gates, T.S.; Nicholson, L.M. & Wise, K.E. (2002). Equivalent-continuum modeling of nano-structured materials. Composites Science and Technology, 62, 1869-1880.

Popov, V.N.; Van Doren, V.E. & Balkanski, M. (2000). Elastic properties of single-walled carbon nanotubes. Physical Review B, 61, 3078-3084.

Popov, V.N. (2004). Carbon nanotubes: properties and application. Materials Science and Engineering R, 43, 61-102

Robertson, D.H.; Brenner, D.W. & Mintmire, J.W. (1992). Energy of nanoscale graphitic tubules. Phyical Review B, 45, 12592-12595.

Ru, C.Q. (2000a). Effective bending stiffness of carbon nanotubes. Physical Review B, 62, 9973-9976.

Ru, C.Q. (2000b). Elastic buckling of single-walled carbon nanotube ropes under high pressure. Physical Review B, 62, 10405-10408

Ruoff, R.S.; Dong, Q. & Liu, W.K. (2003). Mechanical properties of carbon nanotubes: theoretical predictions and experimental measurements. Comptes Rendus Physique, 4, 993-1008.

Sánchez-Portal, D.; Artacho, E. & Soler, J.M. (1999). Ab initio structural, elastic, and vibrational properties of carbon nanotubes. Physical Review B, 59, 12678-12688.

Sunyk, R. & Steinmann, P. (2003). On higher gradients in continuum-atomic modeling. International Journal of Solids and Structures, 40, 6877-6896.

Tadmor, E.; Ortiz, M. & Phillips R. (1996). Quasicontinuum analysis of defects in solids. Philosophy Magazine A, 73, 1529-1563.

Tadmor, E.B.; Smith, G.S.; Bernstein, N. & Kaciras, E. (1999). Mixed finite element and atomistic formulation for complex crystals. Physical Review B, 59, 235-245.

Tersoff, J. (1988). New empirical approach for the structure and energy of covalent systems. Physical Review B, 37, 6991-7000.

Treacy, M.M.J.; Ebbesen, T.W. & Gibson, J.M. (1996). Exceptionally high Young's modulus observed for individual carbon nanotubes. Nature, 381, 678-680.

Van Lier, G.; Van Alsenoy, C.; Van Doren, V. & Geerlings P. (2000). Ab initio study of the elastic properties of single-walled carbon nanotubes and graphene. Chemical Physics Letter, 326, 181-185.

Wang, J.B.; Guo, X.; Zhang, H.W.; Wang, L. & Liao, J.B. (2006a) Energy and mechanical properties of single-walled carbon nanotubes predicted using the higher order Cauchy-Born rule. Physical Review B, 73, 115428.

Wang, J.B.; Guo, X. & Zhang, H.W. (2006b) Nonlinear extension of single-walled carbon nanotubes analyzed by a continuum model based on a higher-order Cauchy-Born rule. Journal of Computational and Theoretical Nanoscience, 3, 798–802.

Wang, J.B.; Guo, X. & Zhang, H.W. (2009a) Higher Order Cauchy-Born Rule Based Study of Chiral Single-walled Carbon Nanotubes. Journal of Computational and Theoretical Nanoscience, 6(7), 1617-1621.

Wang, J.B.; Guo, X. & Zhang, H.W. (2009b) A Revisit of the Bending Stiffness of Graphite Sheet and Single-Walled Carbon Nanotubes. Journal of Computational and Theoretical Nanoscience, 6(10), 2242-2246.

Xiao, J.R.; Gama, B.A. & Gillespie Jr, J.W. (2005) An analytical molecular structural mechanics model for the mechanical properties of carbon nanotubes. International Journal of Solids and Structures, 42, 3075-3092.

Yakobson, B.I.; Brabec, C.J. & Bernholc, J. (1996). Nanomechanics of carbon tubes: instabilities beyond linear response. Physical Review Letters, 76, 2511-2514.

Yu, M.F.; Files; B.S.; Arepalli, S. & Ruoff, R.S. (2000a). Tensile loading of ropes of single wall carbon nanotubes and their mechanical properties. Physical Review Letters, 84, 5552-5555.

Yu, M.F.; Lourie, O.; Dyer, M.J.; Moloni, K.; Kelly, T.F. & Ruoff, R.S. (2000b). Strength and breaking mechanism of multiwalled carbon nanotubes under tensile load. Science, 287, 637-640.

Zhang, H.W.; Wang, L.; Wang, J.B.; Zhang, Z.Q. & Zheng, Y.G. (2008) Torsion induced by axial strain of double-walled carbon nanotubes. Physics Letters A, 372, 3488-3492.

Zhang, P.; Huang, Y.; Gao, H. & Hwang, K.C. (2002a). Fracture nucleation in single-wall carbon nanotubes under tension: a continuum analysis incorporating interatomic potentials. Journal of Applied Mechanics, 69, 454-458.

Zhang, P.; Huang, Y.; Geubelle, P.H. & Hwang, K.C. (2002b). On the continuum modeling of carbon nanotubes. Acta Mechanica Sinica, 18, 528-536.

Zhang, P.; Huang, Y.; Geubelle, P.H.; Klein, P.A. & Hwang, K.C., (2002c). The elastic modulus of single-walled carbon nanotubes: A continuum analysis incorporating interatomic potentials. International Journal of Solids and Structures, 39, 3893-3906.

Zhang, P.; Jiang, H.; Huang, Y.; Geubelle, P.H. & Hwang, K.C., (2004). An atomistic-based continuum theory for carbon nanotubes: analysis of fracture nucleation. Journal of the Mechanics and Physics of Solids, 52, 977-998.

Zhou, G.; Duan, W.H. & Gu, B.L., (2001). First-principles study on morphology and mechanical properties of single-walled carbon nanotube. Chemical Physics Letters, 333, 344-349.

Carbon Nanotubes - Synthesis, Characterization, Applications

Edited by Dr. Siva Yellampalli

ISBN 978-953-307-497-9
Hard cover, 514 pages
Publisher InTech
Published online 20, July, 2011
Published in print edition July, 2011

Carbon nanotubes are one of the most intriguing new materials with extraordinary properties being discovered in the last decade. The unique structure of carbon nanotubes provides nanotubes with extraordinary mechanical and electrical properties. The outstanding properties that these materials possess have opened new interesting researches areas in nanoscience and nanotechnology. Although nanotubes are very promising in a wide variety of fields, application of individual nanotubes for large scale production has been limited. The main roadblocks, which hinder its use, are limited understanding of its synthesis and electrical properties which lead to difficulty in structure control, existence of impurities, and poor processability. This book makes an attempt to provide indepth study and analysis of various synthesis methods, processing techniques and characterization of carbon nanotubes that will lead to the increased applications of carbon nanotubes.

INTECH
open science | open minds

InTech Europe
University Campus STeP Ri
Slavka Krautzeka 83/A
51000 Rijeka, Croatia
Phone: +385 (51) 770 447
Fax: +385 (51) 686 166
www.intechopen.com

InTech China
Unit 405, Office Block, Hotel Equatorial Shanghai
No.65, Yan An Road (West), Shanghai, 200040, China
中国上海市延安西路65号上海国际贵都大饭店办公楼405单元
Phone: +86-21-62489820
Fax: +86-21-62489821

IntechOpen